

Representation learning using RAIN RFID tag backscatter features for material classification in circular economy applications

R. Bhattacharyya and F. Villa-Gonzalez
Auto ID Labs
Massachusetts Institute of Technology
Cambridge, MA 02139
Email: rahul_b, fatimavi@mit.edu

P. Nikitin
Impinj
Seattle, WA 98109
Email: nikitin@ieee.org

Abstract—We present how RAIN RFID power-on-tag-reverse (POTR) features can be used to reliably differentiate between materials having different relative dielectric permittivity (ϵ_r) and effective loss ($\tan(\delta)$). Our approach shows how this is achieved using 15 diverse RAIN RFID tags, having an embedded T-match antenna design, deployed on 7 different material types. We present a data visualization and K-means clustering algorithm that can reliably differentiate between material types with 94% accuracy. We show how our approach is particularly useful at differentiating between materials having very similar ϵ_r but different $\tan(\delta)$. We also demonstrate the technique appears to be robust to reflections, wet inlay adhesives and material thickness via a limited study conducted in a non-idealized warehouse environment. Future research directions are also discussed.

Index Terms—Material identification, representation learning, RAIN RFID tag signal features, circular economy application.

I. INTRODUCTION

Sustainability and waste minimization efforts have contributed to the rise of the circular economy where product and packaging materials are recycled for reuse [1]. Packaging material such as plastics, in particular, are persistent, non-biodegradable and are building up in the environment. Only 9% of plastics in the US are recycled [2]. This is due to a combination of poor quality control at collection, consolidation and transportation to the recycling center [3], and lack of label standardization [4]. Commercial recycling efforts rely on or incentivize [5] users to properly screen items prior to disposal but this can be cumbersome and prone to error.

Optical methods such as barcode or camera data are primarily used for material identification [6]. While these do not need any hardware to be placed on the recycled item, the identification accuracy is dependent on line of sight and lighting conditions. Recently, there has been interest in using wireless material identification technologies. For instance, studies have shown that chipless RFID tags can successfully differentiate between 8 different material types with over 90% accuracy, being 3-16 times faster than optical counterparts [7]. While promising, the nascent nature of chipless RFID technology — associated with a lack of standards and affordable data capture hardware — limits its deployment in practice.

Concurrently, the deployment of passive Ultra-High Frequency (UHF) RFID (also known as RAIN [8]) labels on product packaging is increasing, driven by a substantial decrease in tag costs and recent item level tagging mandates by retailers like Walmart [9]. Research has shown that RAIN RFID technology can offer item-level information that goes beyond basic identification, adding capabilities for material composition sensing, thereby improving sorting accuracy. In this context, Bhattacharyya *et al.* conducted pioneering research on the use of RFID tag antennas for low-cost glass fill-level detection via received signal strength indicator (RSSI) changes [10]. Building upon this, RAIN RFID has also been used for relative permittivity (ϵ_r) and conductivity (σ) estimation and material classification in the last decade (see Table I). For example, Suwalak *et al.* use read range measurements to estimate ϵ_r of construction materials [11], whereas Piccinno *et al.* exploit a self-tunable RFID chip to extract information about the ϵ_r of dielectric materials [12]. Some works estimate the complex permittivity of liquids through frequency and magnitude shifts on the transmitted power and read range curves combined with multivariate regression models [13], [14]. However, all these studies either require custom tag antennas or self-tuning integrated circuits (ICs) (which have a limited impedance tuning range and require the ability to read and record tuning state), restricting their general applicability.

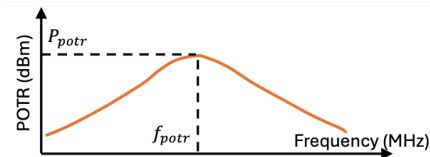


Fig. 1: Threshold POTR of a typical T-matched tag.

There are some research works that use commercial tags (i.e., standardized and general-purpose) for wireless material identification. For instance, the studies by Wang *et al.* and Claucherty *et al.* focus on classifying commercial beverages based on signal changes (e.g., phase, RSSI, power on tag reverse (POTR), power on tag forward (POTF), theoretical

TABLE I: Comparison of reported RAIN RFID-based dielectric property estimation and material classification approaches

Ref.	Materials	Measured parameter(s)	Post-processing	Generalizable? (custom/commercial tag(s))	Complex permittivity
[11]	2 construction materials	Read range	Simulation with prior knowledge of material	No (custom)	No
[12]	10 dielectrics	Sensor code of the chip (capacitance)	Capacitance vs. ϵ_r	No (custom + self-tunable chip)	No
[13]	9 liquids	Frequency shift on the transmitted power and read range	Multivariate regression	No (custom)	Yes
[14]	5 liquids	Frequency and magnitude shift on the read range	Multivariate linear model + power law with reference ϵ_r	No (custom)	Yes
[15]	10 commercial beverages	Phase and Received Signal Strength Indicator (RSSI) changes	Prior knowledge of propagation distance + KNN classifier	No (works for 1 commercial tag)	No
[16]	6 commercial beverages	POTR, POTF, TRRF and radiation pattern	Statistical analysis	No (works for 1 commercial tag)	No
[17]	4 dielectrics	Frequency shift on the POTR	Analytical model + calibration curve	Yes (works for 10 commercial tags)	No
This work	6 materials in packaging	Frequency shift and magnitude on the POTR	K-means clustering and classification	Yes (works for 12 commercial tags)	Yes

read range forward (TRRF) etc.) [15], [16]. However, their approaches are specific to a particular type of commercial tag, with poor performance reported when tested with other tag types. Recently, Nikitin *et al.* demonstrated how shifts in the peak frequency of the POTR, f_{potr} , from any commercial off-the-shelf RAIN RFID tag with an embedded T-matched structure can be used for ϵ_r sensing (c.f. Fig. 1) [17]. Such generalizable development once again brings the utility of RAIN RFID technology for material identification to the forefront.

As demonstrated by Villa-Gonzalez *et al.*, many plastics have similar ϵ_r ranging between 2.2 - 2.8 [18], but exhibit differences in material loss ($\tan(\delta)$) ranging from 0.0003 - 0.006. This paper explores an opportunity to expand Nikitin's work to examine the effect of $\tan(\delta)$ on POTR curve characteristics, such as POTR peak magnitude, P_{potr} , of generic commercial tags as an additional feature for material identification.

The contribution of this work is two fold. First, we experimentally demonstrate how changes in P_{potr} can be correlated to effective $\tan(\delta)$ repeatably and reliably using 6 different material types (and air) with 12 different RAIN RFID tags. We specifically demonstrate our ability to differentiate between materials having very similar ϵ_r but different $\tan(\delta)$. Second, we demonstrate how unsupervised machine learning techniques, such as K-means, can be used to automatically differentiate between and classify these materials, using P_{potr} and f_{potr} data, with high accuracy. Finally, the utility of this technique in a practical, non-idealized setting is examined.

The rest of the paper is organized as follows. Section. II discusses our hypothesis of how f_{potr} and P_{potr} can be used to detect the ϵ_r and $\tan(\delta)$ of different materials. Section. III presents the tags used, materials tested and hardware setup. Section. IV discusses the data collected, how it is processed for visualization as well as the results of implementing a k-means clustering algorithm for material identification. Section. V then demonstrates the robustness of our approach in a practical, non idealized environment. Finally, Section. VI presents the main conclusions and future research directions.

II. HYPOTHESIS FOR MATERIAL LOSS DETECTION

Previous studies have characterized the effect of dissipative materials on antenna performance. For lossy dielectrics with high $\tan(\delta) = \epsilon''/\epsilon'$, the increased imaginary part of the complex dielectric constant (ϵ'') reduces the quality factor (Q) of any antenna. This manifests as a reduction of peak radiation conductance and increase in operational bandwidth [19]–[21]. RFID tag antennas may exhibit different geometries, but the operating principle of all T-matched designs is based on a coupled loop-dipole configuration. As derived by Nikitin *et al.* in [22], the POTR of any tag is directly proportional to the conductance of the tag antenna. We therefore expect a similar relationship between P_{potr} and $\tan(\delta)$.

To test this hypothesis, we consider a typical RAIN RFID small 40x15 mm inlay, Impinj AR-61F with Impinj Monza R6 IC (c.f. Table II) and place it on polytetrafluoroethylene (PTFE) and glass (see Table III), two materials typically found in recycling chains. Both material samples were 4 mm thick in order to avoid variations in effective ϵ_r . POTR measurements utilized the Voyantic Tagformance Broadband Kit [23]. Fig. 2 illustrates the POTR curves for the AR-61F tag placed on the two materials and in air. As outlined in [17], f_{potr} decreases as ϵ_r increases. In addition, we also notice a decrease in P_{potr} as $\tan(\delta)$ increases illustrating that there may be credence to our hypothesis. However, from Fig. 6 in [17], we note that the relationship between P_{potr} and $\tan(\delta)$ may not be consistent across tags and needs to be investigated further in a systematic manner.

In the next section, we therefore validate the repeatability and reliability of our hypothesis more exhaustively by measuring the POTR performance of 12 RAIN RFID tags, with an embedded T-match structure, on 6 different types of materials (and air) with different ϵ_r and $\tan(\delta)$ values. In addition, the accuracy of using f_{potr} and P_{potr} as features to train a k-means classifier to automate material identification will be examined.

III. EXPERIMENTAL SETUP

In this section, we discuss the tags and types of materials used in the study and present the experimental setup.

A. RAIN RFID tags

Table II illustrates all the T-matched tags considered in this study. The dimensions and the IC are also listed. As observed, the tag antenna designs vary significantly as do the size and attached ICs. T-matched designs represent most of RAIN RFID tags on market, including ARC-certified tags [24], and should be adequate to evaluate the efficacy of our hypothesis experimentally. The Beontag models (A701, H61 and E702) are used twice, resulting in 15 diverse tags. In the second test, a judicious amount of adhesive tape was used to attach the tags to the materials, in order to evaluate the effect of their typical attachment to packaging.

B. Materials tested

We use the reference material kit provided by Voyantic [25]. The materials and their dielectric properties are summarized in Table III. The ϵ_r values vary from 2.05 to 7.11 and $\tan \delta$

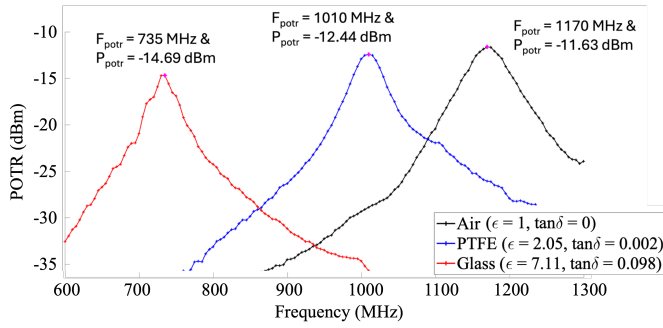
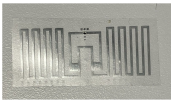
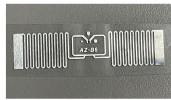


Fig. 2: f_{potr} and P_{potr} for the AR-61F tag in air and when placed on 4 mm thick PTFE and glass materials.

TABLE II: T-matched antenna-based commercial RAIN RFID tags considered in this study

Tag	Model	Size (mm)	IC	Image	Tag	Model	Size (mm)	IC	Image
1	Beontag A701	42 x 16	Impinj Monza M750		7	Arizon AZ-B6	85 x 25	Impinj Monza R6	
2	Arizon AZ-MR71	42 x 16	Impinj Monza M730		8	Tageos EOS-241	42 x 16	NXP UCODE 9	
3	Arizon AR-61F	40 x 15	Impinj Monza R6		9	Invengo Bullet	41 x 15	Impinj Monza R6	
4	Beontag H61	50 x 30	Impinj Monza R6		10	Invengo Butterfly	50 x 30	Impinj Monza R6	
5	Beontag E702	70 x 14	Impinj Monza M730		11	Checkpoint Vortex	42 x 16	Impinj Monza M750	
6	Arizon AZ-HR7G	71.5 x 18	Impinj Monza M730		12	Avery Denison AD-386	50 x 30	Impinj Monza M730	

values vary from 0.0002 to 0.0717. In addition, materials such as POM and PVC, or glass and rubber are of particular interest, given the very similar ϵ_r but different $\tan \delta$ values. All materials have a 130x130 mm footprint and are 4 mm thick (see Fig. 3(A)).

TABLE III: Summary of material properties in Voyantic kit

Material	ϵ_r	$\tan(\delta)$
Cardboard (CB)	2.57	0.0717
PTFE	2.05	0.0002
Glass	7.11	0.0098
Polyvinyl chloride (PVC)	3	0.0079
Acetal (POM)	2.96	0.045
Rubber	6.73	0.0247

C. Reader hardware and test setup

We make use of the Voyantic Tagformance Broadband kit [23], which is capable of testing tags in the 600-1300 MHz band. The RAIN tag under test (TUT) (see Section III-A) is placed on the material under test (MUT) (see Section III-B) and placed at a distance of 0.5 m from the reader antenna (c.f. Fig. 3(B)). In order to avoid an air gap and make the TUT flush with the MUT surface, RF transparent foam is gently wedged between the reader and tag antennas to apply a uniform pressure on the tag. Tests are also conducted in an anechoic chamber so as to minimize the effect of environmental reflections (c.f. Fig. 3(C)). For each TUT and MUT, a POTR measurement is conducted and f_{potr} and P_{potr} are extracted from curves similar to the ones in Fig. 2.

IV. RESULTS

In this section, we discuss the data processing, visualization and results of applying machine learning for material classifi-

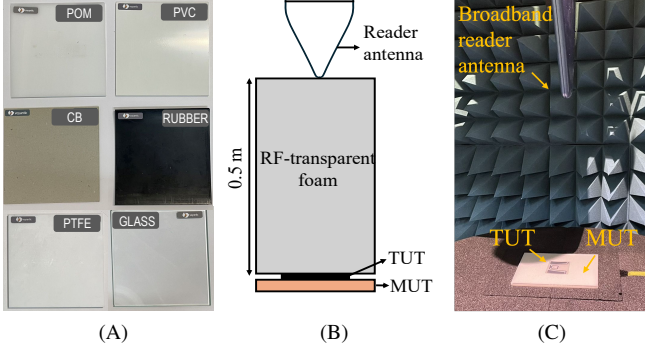


Fig. 3: Experimental setup: A) materials B) diagram C) test environment (RF-transparent foam omitted for visibility).

cation.

A. Data processing and visualization

The first step in data processing is to perform normalization of the data. Table IV shows (f_{potr} and P_{potr}) across two selected tags for the 6 materials and air ($\epsilon_r = 1.00006$, $\tan(\delta) = 0$). It is clear that the relative shifts in (f_{potr} and P_{potr}) need to be compared as the absolute values will clearly differ across tags. This can also be seen in Table III in [17].

TABLE IV: f_{potr} and P_{potr} values across two different tags.

Material	Tag 4		Tag 3	
	f_{potr} (MHz)	P_{potr} (dBm)	f_{potr} (MHz)	P_{potr} (dBm)
Air	975	-12.17	1170	-11.6
Cardboard (CB)	885	-14.69	1000	-16.1
PTFE	860	-11.15	1010	-12.4
PVC	810	-11.71	935	-13.7
POM	810	-14.55	925	-16.4
Rubber	665	-11.03	730	-15.4
Glass	665	-10.61	735	-14.7

First, a simple normalization method is applied. For a particular TUT test, denoted as i , f_{potr} and P_{potr} are normalized for each MUT, j , relative to air ($j = 1$) such that:

$$f_{potr,ij}^N = \frac{f_{potr,ij}}{f_{potr,i1}}, P_{potr,ij}^N = \frac{P_{potr,ij} - P_{potr,i1}}{P_{potr,i1} - P_{potr,i1}} \quad (1)$$

where $i = 1, 2, \dots, 15$ and $j = 1, 2, \dots, 7$.

The advantage of this method is that only the performance of the TUT in air is needed for calibration purposes. Fig. 4 illustrates the normalized f_{potr}^N and P_{potr}^N clusters for all 7 MUTs for each of the 15 TUT tests. While there are some spatial similarities between MUTs, it may be difficult for an automated algorithm such as a machine learning classifier to reliably differentiate between them due to the regions of overlap between cluster points.

In order to maximize the spacing between clusters, we apply *min-max* scaling and represent all MUT clusters on a common [0,1] scale using the highest $f_{potr,i}^{max}$ and $P_{potr,i}^{max}$ and lowest

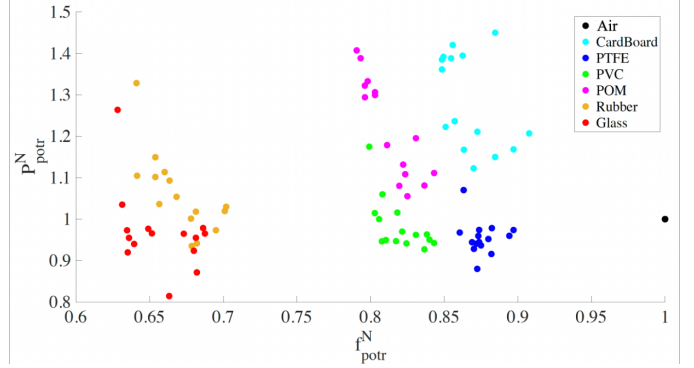


Fig. 4: MUT representation when f_{potr} and P_{potr} are normalized relative to air for each TUT.

$f_{potr,i}^{min}$ and $P_{potr,i}^{min}$ values across all MUTs ($j = 1, 2, \dots, 7$) for a given TUT test, i , as follows:

$$f_{potr,ij}^N = \frac{f_{potr,ij} - f_{potr,i}^{min}}{f_{potr,i}^{max} - f_{potr,i}^{min}}, P_{potr,ij}^N = \frac{P_{potr,ij} - P_{potr,i}^{min}}{P_{potr,i}^{max} - P_{potr,i}^{min}} \quad (2)$$

As observed in Fig. 5, the cluster points become much more amenable for automated classification. The disadvantage of *min-max* scaling is that a calibration set of each MUT for a particular TUT is necessary in order position the cluster point in the [0,1] space. Nevertheless, the trends in the data are logically sound. For instance, materials with lower ϵ_r are closer to $f_{potr}^N = 1$ and materials with lower $\tan(\delta)$ are closer to $P_{potr}^N = 1$. Moreover, it is possible to differentiate between materials having similar ϵ_r and very different $\tan(\delta)$ and seen by the clusters formed by PVC (green) and POM (magenta).

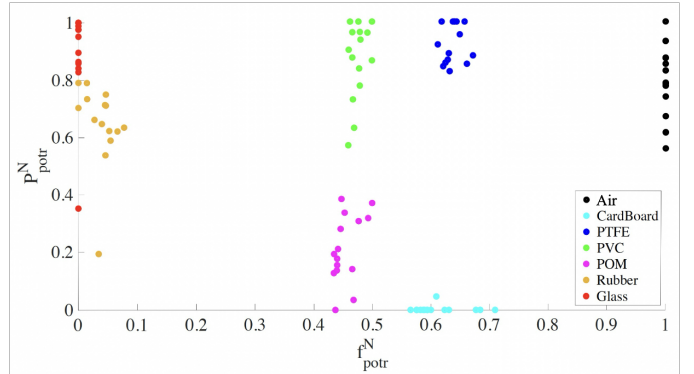


Fig. 5: MUT representation after *min-max* and common [0,1] scaling.

Finally, we apply Fisher Linear Discriminant Analysis (LDA) [26] to the cluster data so as to maximize the inter-cluster variation while minimizing the intra-cluster variation. The new projected data is shown in Fig. 6.

B. K-means clustering and classification

While the color coded clusters in Fig. 6 appear separable to the human eye, it is necessary to see how well a machine learning classifier is able to discern between them. We apply the

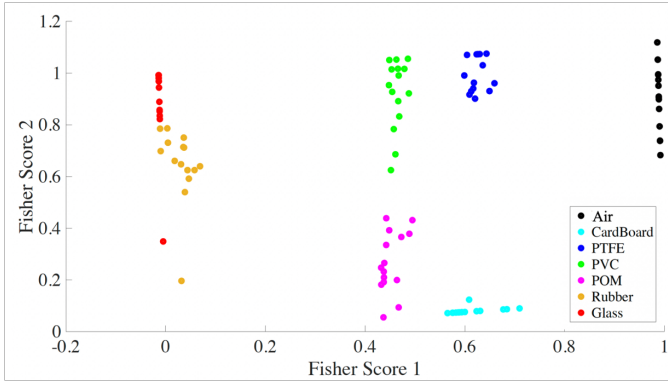


Fig. 6: MUT representation after Fisher LDA transformation

K-means clustering algorithm on the Fisher LDA transformed data to test this ability [26]. We only specify the number of clusters as prior information to the clustering algorithm. We also specify the centroids of the clusters as starting seed values.

Fig. 7 and Table V show the results of clustering. The algorithm is able to achieve 94.28% classification accuracy, indicating the promising potential of using machine learning techniques for material classification.

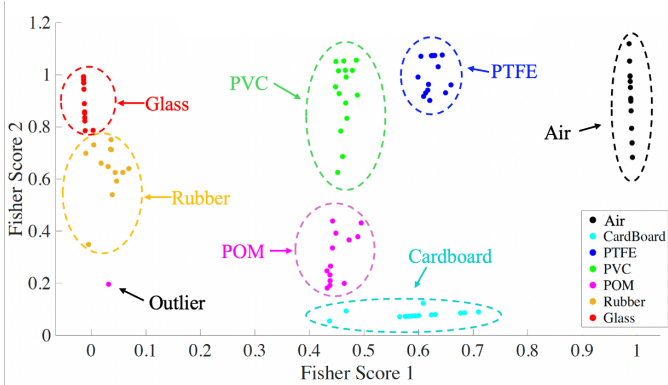


Fig. 7: K-means clustering results on LDA transformed data.

TABLE V: Confusion matrix of K-means classification

Ground truth	Prediction						
	Air	CB	PTFE	PVC	POM	Rubber	Glass
Air	15	0	0	0	0	0	0
CB	0	15	0	0	0	0	0
PTFE	0	0	15	0	0	0	0
PVC	0	0	0	15	0	0	0
POM	0	2	0	0	13	0	0
Rubber	0	0	0	0	1	12	2
Glass	0	0	0	0	0	1	14

V. PRACTICAL STUDY

We conduct a study where the Voyantic system is deployed in a non idealized real-life environment; in this case an open warehouse environment (see Fig. 8(A)). The MUT is deployed in front of the reader antenna at a distance of 55 cm. The RFID tag on the MUT was placed facing the reader antenna.

Fig. 8(B) shows the materials considered in this study, which are common items recycled by households. The dielectric material properties of these items is shown in Table VI. We made use of 6 RAIN RFID tags in the testing: tags 1, 4 and 5 in Table II and tags 13-15 in Table VII. The latter were chosen because, unlike most of the tags in Table II, they are wet inlays, which are more likely to be encountered in practice as they are easily deployed on product packaging.

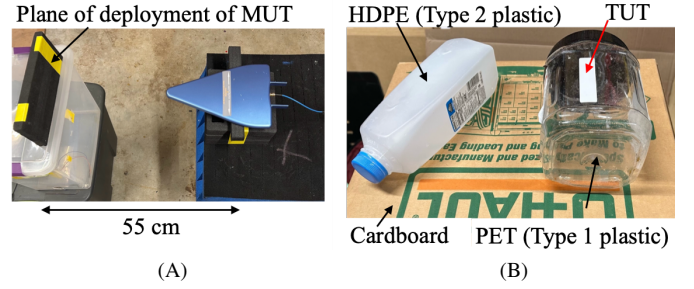


Fig. 8: (A) Non idealized testing setup. (B) Recyclable materials used in this study.

TABLE VI: Dielectric properties of recyclable materials

Material	ϵ_r	$\tan(\delta)$
Cardboard	2.57	0.0717
HDPE	2.3	0.0005
PET	2.8	0.003

TABLE VII: Wet inlays considered in real-life testing

Tag	Model	Size (mm)	IC	Image
13	Avery Dennison AD-321	41 x 16	Impinj Monza R6	
14	Avery Dennison AD-226	95 x 8	NXP G2IM	
15	Avery Dennison Smartrac Belt	73 x 17	Impinj Monza R6	

Fig. 9 shows the Fisher LDA transformed clusters obtained by following the procedure outlined in Section IV. The material clusters are correctly classified with 100% accuracy indicating that this technique holds promise in non-idealized settings. Furthermore, the cluster trends are also as expected. Higher ϵ_r are closer to the left hand side of the graph while higher $\tan(\delta)$ are closer to bottom.

Moreover, there are some additional considerations that are promising for the practical deployment of this technique. First, the dielectric detuning caused by the adhesives and paper by the three wet inlays used in this test is not significant enough to compromise test performance. Second, the three

recyclable MUT materials were of different thicknesses (unlike the standardized materials considered in Section III-B).

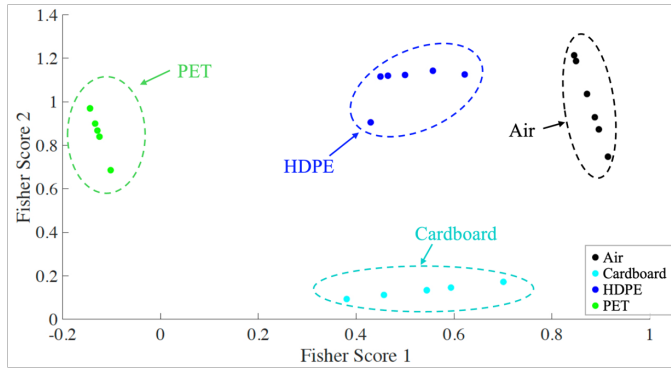


Fig. 9: Fisher LDA transformed MUT clusters using the 6 RAIN test tags.

VI. CONCLUSIONS AND FUTURE WORK

We present a data visualization and K-means clustering algorithm that uses RAIN RFID tag f_{potr} and P_{potr} to differentiate between and classify materials with different ϵ_r and $\tan(\delta)$ values. We demonstrate this using 6 materials of known permittivity values (plus air) and 12 RAIN RFID tags having an embedded T-match antenna design, with 4 different ICs. We specifically show the ability to differentiate between materials having very similar ϵ_r but different $\tan(\delta)$ such as POM and PVC or rubber and glass. Overall the method achieves 94.28% accuracy in our testing. An additional study in a non-idealized warehouse-like environment using 3 common recyclable materials and 6 tags shows that the technique works with 100% classification accuracy. Moreover, complicating factors such as adhesives and paper in wet inlays do not unduly compromise performance. Our approach therefore shows good promise, contributing to the circular economy by identifying tagged discarded packaging material for reuse and recycling.

As future work, we plan to examine the applicability of this technique to RAIN RFID tags without a T-match structure. Second, we would like to develop a lower-cost version of the Tagformance reader based on existing parallel research efforts [27] and understand the trade-off between lower cost electronics and classification accuracy. Third, we plan to examine the effect of practical considerations such as different material thicknesses, reading the tag through the material, exposure to moisture and different humidity conditions and situations where multiple tags and materials are in close proximity to one another. Finally, we would also like to expand the approach to additional materials, such as other types of plastics and bottles with oils, alcohols and aqueous solutions.

REFERENCES

- [1] K.L. Sven et al., "Promoting circular economy transition: A study about perceptions and awareness by different stakeholders groups," *Journal of Cleaner Production*, vol. 316, p. 128166, 2021.
- [2] J.P. Harrison et al., "Biodegradability standards for carrier bags and plastic films in aquatic environments: A critical review," *R. Soc. open sci.*, vol. 5, p. 171792, 2018.
- [3] R. Cho, "Recycling in the U.S. is broken. How do we fix it?." Brochure: <https://blogs.ei.columbia.edu/2020/03/13/fix-recycling-america/>, 2013. Accessed on: Sept. 28, 2022.
- [4] E. Moss and R. Harris, "Can I recycle this? A global mapping and assessment of standards, labels and claims on plastic packaging," tech. rep., UN Env. Prog. & Cons. Int., 2020.
- [5] MeCycle, "Make your recycling matter." [Online]. Available: <https://www.me-cycle.com/>. Accessed on: Sept. 28, 2022.
- [6] D. Ziouzos and M. Dasygenis, "A smart recycling bin for waste classification," *Panhellenic Conference on Electronics Telecommunications (PACET)*, pp. 1–4, 2019.
- [7] D. Tellbach et al., "Wireless material identification in the recycling chain using chipless RFID tags," *IEEE Sensors Journal*, vol. 23, no. 13, pp. 14976–14987, 2023.
- [8] RAIN Alliance, "What is RAIN Alliance?." [Online]. Available: <https://therainalliance.org/>. Accessed on: Jan. 20, 2025.
- [9] N. Eaton, Impinj Insights, "Walmart expands RFID mandate: What it means for RAIN RFID in retail." [Online]. Available: www.impinj.com/library/blog/walmart-makes-big-rfid-commitment-with-sweeping-tag-mandate. Accessed on: Jan. 16, 2025.
- [10] Bhattacharyya, R. et al., "RFID tag antenna based sensing: Does your beverage glass need a refill?," in *IEEE Int. Conf. on RFID*, pp. 126–133, 2010.
- [11] R. Suwalak et al., "Determination of dielectric property of construction material products using a novel RFID sensor," *PIER*, vol. 130, pp. 601–617, 2012.
- [12] F. Piccinno et al., "Exploiting self-tunable RFID chips for wireless sensing of permittivity to enable passive low-cost food-quality monitoring systems," in *IEEE 13th Int. Conf. on RFID Tech. and App. (RFID-TA)*, pp. 45–48, 2023.
- [13] V. Makarovaite et al., "Passive wireless UHF RFID antenna label for sensing dielectric properties of aqueous and organic liquids," *IEEE Sensors Journal*, vol. 19, no. 11, pp. 4299–4307, 2019.
- [14] S. López-Soriano et al., "Remote identification of liquids using absorbent materials: a passive UHF RFID-based method," *IEEE Sensors Journal*, pp. 1–1, 2025.
- [15] J. W. et al., "Simultaneous material identification and target imaging with commodity RFID devices," *IEEE Trans. on Mobile Computing*, vol. 20, no. 2, pp. 739–753, 2021.
- [16] E. Claucherty et al., "Effect of beverage composition on Radio Frequency Identification (RFID) performance using Polyethylene Terephthalate (PET) bottles for smart food packaging applications," *Foods (Basel, Switzerland)*, vol. 13, no. 5, p. 643, 2024.
- [17] P. Nikitin et al., "Dielectric sensing using T-matched RAIN RFID tags," in *IEEE Int. Conf. on RFID*, pp. 42–47, 2023.
- [18] Villa-Gonzalez, F. et al., "Single and bulk identification of plastics in the recycling chain using chipless RFID tags," in *2021 IEEE Int. Conf. on RFID*, pp. 1–8, 2021.
- [19] A. Yaghjian and S. Best, "Impedance, bandwidth, and Q of antennas," *IEEE Trans. on Ant. and Prop.*, vol. 53, no. 4, pp. 1298–1324, 2005.
- [20] E. E. Altshuler et al., "An electrically small genetic antenna immersed in a dielectric," in *2007 IEEE Antennas and Propagation Society International Symposium*, pp. 6003–6006, 2007.
- [21] R. Bhattacharyya et al., "Towards low-cost, wireless blood anomaly sensing: An RFID-based anemia detection sensor," in *IEEE Int. Conf. on RFID*, pp. 189–196, 2015.
- [22] P. Nikitin, J. Kim, and K. Rao, "RFID tag analysis using an equivalent circuit," in *2021 IEEE Int. Symp. APS/URSI*, pp. 167–168, 2021.
- [23] "Voyantic Tagformance Pro." [Online]. Available: voyantic.com/lab/tagformance-pro/. Accessed on: Jan. 16, 2025.
- [24] Impinj, "RAIN RFID Tags from Impinj Partners." [Online]. Available: <https://www.impinj.com/partners/products/partner-tags?pagesize=500>. Accessed on: Jan. 21, 2025.
- [25] Voyantic, "Reference Material Set." [Online]. Available: <https://voyantic.com/lab/tagformance-pro/accessories/>. Accessed on: Jan. 17, 2025.
- [26] R. Duda et al., *Pattern Classification (2nd Ed.)*. Wiley Interscience, 2000.
- [27] N. Barbot et al., "Simple low cost open source UHF RFID reader," *IEEE Journal of Radio Frequency Identification*, vol. 7, pp. 20–26, 2023.